Influence of pumping operational schedule on solute concentrations at a well in randomly heterogeneous aquifers

Arianna Libera [a,*], Felipe P. J. de Barros [a,1], Alberto Guadagnini [b,c,2]

[a] *Sonny Astani Department of Civil and Environmental Engineering, University of Southern California, Kaprielian Hall, 3620 S. Vermont Avenue, Los Angeles, CA 90089, USA*

[b] *Dipartimento di Ingegneria Civile e Ambientale, Politecnico di Milano, Piazza L. Da Vinci 32, 20133 Milano, Italy*

[c] *Department of Hydrology and Atmospheric Sciences, University of Arizona, Tucson, AZ 85721, USA*

** Tel.: +1 213 740 0603*

E-mail address: libera@usc.edu

[1] *Corresponding author. Tel.: +1 213 740 6130*

E-mail address: fbarros@usc.edu (F. P. J. de Barros)

[2] *Tel.: +39 02 2399 6263*

E-mail address: alberto.guadagnini@polimi.it

Abstract

We investigate the way diverse groundwater extraction strategies affect the history of solute concentration recovered at a pumping well while taking into account random spatial variability of the system hydraulic conductivity. Considering the joint effects of spatially heterogeneous hydraulic conductivity and temporally varying well pumping rates leads to a realistic evaluation of groundwater contamination risk at the pumping well location. We juxtapose the results obtained when the pumping well extracts a given amount of water operating (a) at a uniform pumping rate and (b) under a transient regime. The analysis is performed within a numerical Monte Carlo framework. Our results show that contaminant concentration breakthrough curves (BTCs) at the well are markedly affected by the transient pumping strategy according to which the well is operated. Our results document the occurrence in time of multiple peaks in the mean and variance of flux-averaged concentrations at the extraction well operating at a transient rate. Our findings suggest that lowest and largest values of mean and variance of flux-averaged concentration at the well tend to occur at the same time. We show that uncertainty associated with detected BTCs at the well increases for pumping regimes displaying a high degree of temporal variability. As such, the choice of the type of engineering control to the temporal sequence of pumping rates could represent a key factor to drive quantification of uncertainty of the contaminant concentration detected at the well. It is documented that pumping rate fluctuations induce a temporally oscillating risk pattern at the well, thus suggesting that the selection of a dynamic pumping regime has a clear influence on the temporal evolution of risk at the well.

1. Introduction

Pumping wells are widely employed for groundwater supply in the context of urban, agricultural, and industrial activities. Water management agencies typically schedule groundwater extraction through a well-defined temporal sequence of pumping rates to maximize benefits to anthropogenic activities and minimize the environmental footprint of the withdrawal process. The temporal dynamics of well pumping operations induce changes in the subsurface flow field which in turn can affect spreading and mixing of contaminant plumes. A key challenge is to provide estimates of contaminant concentration at an environmentally sensitive location while accounting for the joint effect of the temporal dynamics of an operating pumping well and the (typically uncertain) spatial variability of the hydrogeological properties of the subsurface reservoir within which a potentially harmful solute is residing and migrating.

The effect of the spatial variability of hydraulic properties of aquifers, such as hydraulic conductivity, on contaminant transport has been broadly studied (e.g., *Gelhar*, 1993; *Dagan and Neuman*, 1997; *Rubin*, 2003). Due to the high cost of data acquisition campaigns and limited financial resources, a highly detailed characterization of the spatial distribution of hydrogeological attributes (e.g., hydraulic conductivity) of an aquifer system at the field scale of interest is virtually unfeasible. As a consequence, this lack of knowledge leads to uncertainty associated with predicted values of contaminant concentration at environmentally sensitive and strategically valuable locations, such as pumping wells. As noted in the following, while a considerable amount of published works address the analysis of contaminant transport under steady-state pumping, the way a given time-varying pumping schedule affects contaminant plume behavior in heterogeneous aquifers is tackled only marginally.

Uncertainty in the quantification of the extent of pumping well protection regions (both in terms of well catchment and time-related capture zones) in the presence of random spatial distributions of aquifer parameters and under the assumption of steady-state background groundwater flow to which one or more wells extracting a constant flow rate are superimposed has been addressed, amongst others, by *Cole and Silliman* (1997), *Varljen and Shafer* (1991), *Franzetti and Guadagnini* (1996), *Vassolo et al*. (1998), *van Leeuwen et al.* (1998, 2000), *Guadagnini and Franzetti* (1999), *Riva et al.* (1999), *Feyen et al.* (2001) through numerical Monte Carlo simulations (unconditional or conditional on data). *Stauffer et al.* (2002) performed a theoretical analysis based on first-order approximation and a Lagrangian approach to estimate the uncertainty associated with the delineation of well catchments in the presence of a spatially variable random hydraulic conductivity field. *Lu and Zhang* (2003) used a Lagrangian framework for the study of time-related capture zones in spatially randomly heterogeneous aquifers. *Riva et al.* (2006) used stochastic moment equations to analyze the uncertainty associated with well catchments. The work of *de Barros at el.* (2013) addressed the value of hydrogeological information to assess the risk associated with pollution of an operating pumping well. *Molson and Frind* (2012) applied the concept of mean life expectancy (i.e., the time between plume detection and plume capture by a well) and capture probability to delineate well capture zones. The life expectancy approach constitutes an alternative to delineate time-of-travel capture zones for wellhead protection. *Pedretti and Fiori* (2013) developed an analytical solution of contaminant transport in heterogeneous porous media under purely convergent flow to analyze solute breakthrough curves (BTCs) at the well. *Indelman and Dagan* (1999) analyzed the spreading of a contaminant plume injected in a heterogeneous formation through a well and advected by a steady-state groundwater velocity.

Only a limited number of works consider the impact of transient flow regimes on the delineation of capture zones or wellhead protection areas (WHPA). Amongst these, *Ramanarayanan et al.* (1995) used numerical models to delineate the WHPA of two municipal wells under the influence of nearby irrigation wells. Their conclusion was that seasonal variation in pumping rates affected the water table depth and the extent of a target time-related well capture zone. In this sense, significant seasonal variations in pumping operations should be explicitly embedded in a procedure for WHPA delineation. *Reilly and Pullock* (1996) employed a numerical flow model and a particle tracking method to investigate the effects of external stresses, i.e. recharge (that is typically cyclic over time), on the area contributing recharge to the wells. They observed that the ratio between the mean travel time of the solute to the well and the period of cyclic stress can provide a quantification of the importance of considering the transient effects of a cyclic recharge. The authors noted that: (*a*) approximating the system behavior through an average steady-state condition yields results which are similar to those obtained by considering the actual transient pattern of recharge when the above ratio is much larger than one; and (*b*) considering transient flow conditions is important to characterize the proper behavior of solutes released in the proximity of the boundary of the well. *Jacobson et al.* (2002) incorporated the effects of uncertainty in the transmissivity and the magnitude and direction of the hydraulic head gradient in the steady-state analytical solution obtained by *Bear and Jacobs* (1965) for capture zones delineation. These authors observed that uncertainty in the magnitude of the mean regional flow propagates to the uncertainty in the length (along the direction of the regional flow) of the time-dependent capture zone. Otherwise, uncertainty in the mean direction of the background flow influences the uncertainty in the maximum width (along a direction normal to the average regional flow) of the capture zone. *Festger and Walter* (2002) analyzed the same problem through a semi-analytical approach. They concluded that temporal variations in the direction of the background natural hydraulic gradient typically cause an expansion of a given capture zone when compared against its steady-state counterpart, the opposite being observed in some specific cases (e.g., in the presence of moderate directional variations and large gradient magnitudes). *Neupauer et al.* (2014) investigated the effects of aquifer heterogeneity on the spreading of a plume of conservative solute which is advected within a temporally variable flow field induced by engineered injection and extraction sequences. Other authors, e.g. *Assouline et al.* (2006), illustrate that transient effects associated with high-frequency irrigation affect solute and water regimes and residence times under partially saturated conditions.

Additional examples of contaminant transport studies which incorporate the effects of transient pumping strategies include the works of *Chang et al.* (1992), who simulated unsteady flow to optimize time-varying pumping rates for groundwater remediation; *Vesselinov* (2007), who studied the influence of transient flow and of uncertainty in longitudinal and transverse dispersivities on the delineation of well capture zones; *Chen et al.* (2012), who evaluated solute transport in divergent radial flow fields created by multistep pumping; and *Leray et al*. (2014), who detected the occurrence of non-negligible solute concentrations at a pumping well following induction of a transient flow field by the instantaneous activation of the well. In contrast to our work, *Leray et al*. (2014) did not investigate the uncertainty of the contaminant concentrations recovered at the well.

Notably, in this broad context, the effects of a temporally varying pumping regime on contaminant solute BTCs detected at the location of the pumping well operating in a heterogeneous aquifer has not been systematically addressed. Our work is then geared towards a first exploration of the joint effects of (*a*) random spatial variability of hydraulic conductivity and (*b*) transient flow regime, as induced by a temporally varying pumping schedule, on this key feature of contaminant transport. These results will then be employed in the context of risk quantification at the well, which is considered as a sensitive strategic location with social and economic value. Risk is here quantified in terms of the probability that an established threshold for the concentration of a target chemical species is exceeded. As such, the objective of our study is directly related to the assessment of risks associated with contamination of drinking water extracted at the well (see. e.g., the works of *Hashimoto et al*., 1982; *Frind et al*., 2006; *de Barros et al.*, 2009; and *Enzenhoefer at al*., 2012).

2. Problem formulation

We consider fully saturated groundwater flow taking place in a heterogeneous porous medium characterized by a spatially variable isotropic random transmissivity field $T(\boldsymbol{x})$ [L^2/T], uniform porosity φ [-], constant thickness b [L] and a uniform-in-the-average natural base flow Q_0 [L^3/T]. The location vector is here expressed as $\boldsymbol{x} = (x, y)$, in a Cartesian coordinate system. Figure 1 depicts a sketch of the domain and problem we study.

The log transmissivity $Y(\boldsymbol{x}) = \ln[T(\boldsymbol{x})]$ is assumed to be a normally distributed and a weakly stationarity correlated random field, which is fully described by its mean, m_Y, and covariance function, C_Y (e.g., *Rubin*, 2003). The covariance function is statistically isotropic and characterized by the variance of $Y(\boldsymbol{x})$, denoted by σ_Y^2, and its (isotropic) correlation scale λ [L]. A pumping well located at $\boldsymbol{x_w} = (x_w, y_w)$ operates with pumping rate $Q_w(t)$ [L^3/T], with t [T] denoting time. Therefore, the flow field is described by the depth-averaged saturated groundwater flow equation:

$$S\frac{\partial h(\boldsymbol{x},t)}{\partial t} = \nabla \cdot [T(\boldsymbol{x})\nabla h(\boldsymbol{x},t)] + Q_w(t)\delta(\boldsymbol{x}-\boldsymbol{x}_w); \qquad (1)$$

where h [L] is the hydraulic head, S [-] corresponds to storativity and δ is the Dirac delta function. Fixed hydraulic head values are imposed on the west (left) and east (right) boundaries and no-flow boundary conditions are set on the north and south boundaries of the domain, resulting in a uniform mean base flow along the *x*-direction (Figure 1).

A tracer with initial uniform concentration c_0 [M/L^3] is instantaneously injected at time t_0 [T] within a region of area A_0 [L^2]. Transport of the tracer plume is described by the standard advection-dispersion equation:

$$\frac{\partial c(\boldsymbol{x},t)}{\partial t} = -\boldsymbol{v}(\boldsymbol{x},t)\cdot\nabla c(\boldsymbol{x},t) + \nabla\cdot[\boldsymbol{D}\nabla c(\boldsymbol{x},t)]; \qquad (2)$$

$$c(\boldsymbol{x},t_0) = c_0 \text{ for } \boldsymbol{x} \in A_0.$$

Here, c [M/L^3] is solute resident concentration, $\boldsymbol{v} = \boldsymbol{q}/\varphi$ [L/T] is effective velocity (and $\boldsymbol{q}$ [L/T] is the specific discharge) and $\boldsymbol{D}$ [L^2/T] is the local-scale dispersion tensor with longitudinal component D_x and transverse component D_y.We consider that solute transport takes place sufficiently far away from the boundaries (Figure 1). Once we obtain the space-time distribution of the concentration we evaluate the flux-averaged concentration C [M/L^3] at the pumping well (*Kreft and Zuber*, 1979) and obtain the solute BTC. Details related to the computational method used to evaluate (1) and (2) are provided in Section 3.

Equations (1) and (2) are expressed in dimensional form. In this work, we will analyze our results in terms of relevant dimensionless groups. We start by the following functional relationship between system parameters and state variables of interest (see also, e.g., *Franzetti and Guadagnini*, 1996):

$$f_1(t, x, y, T, b, q_0, C, Q_w, \varphi, \boldsymbol{D}) = 0; \quad (3)$$

with q_0 [L/T] being the imposed uniform Darcy's background groundwater specific discharge. We consider q_0, Q_w, b and φ as deterministic in our analysis. The following relationship between dimensionless quantities can then be written under the assumption that φ and $\boldsymbol{D}$ are constant:

$$f_2\left(\frac{tq_0^2 b}{Q_w}, \frac{xq_0 b}{Q_w}, \frac{yq_0 b}{Q_w}, \frac{T}{q_0 b}, \frac{C}{C^*}\right) = 0. \quad (4)$$

Note that the dependence on a typical Péclet number would appear in (4) in case one would consider analyzing the interplay between advective and dispersive processes in the system (see Sections 3 and 4.4 for a discussion on this aspect).

The reference concentration C^* in (4) is taken as the contaminant concentration limit value for a target chemical species. The value of the latter is established, for example, by regulatory bodies/agencies. In the regulatory context, this contaminant concentration limit can represent the *Maximum Contaminant Level* for drinking water. Note that Q_w in (4) indicates the constant pumping well extraction rate. In this work, the constant pumping rate, which is selected in the steady-state setting, coincides with the average (over the temporal window of well operation) of the pumped flow rate in the transient scheme (see Section 3). Adopting the constant (in time) extraction rate is then a natural choice to normalize the various terms in (4) for both the steady-state and transient settings analyzed.

Due to the randomness of $Y(\boldsymbol{x})$, the feedback between a transient pumping regime and contaminant breakthrough curves must be studied in a stochastic framework. Section 3 provides details of the computation of the flux-averaged concentration at the well.

3. Methodology

We consider a rectangular solute source, with longitudinal (along direction x) dimension L_1 and transverse (along direction y) dimension L_2, within which solute is instantaneously released in the system (i.e. the area of the source is $A_0 = L_1 \times L_2$, see Figure 1). A pumping well is located at a distance L (measured along the x-direction) from the contaminant source and aligned with the source centroid location. The computational domain has size $\Omega = [(x, y)| x \in (0, L_x); y \in (0, L_y)]$ with $L_x = 170$ m and $L_y = 150$ m. We considered a unit thickness aquifer in all simulations.

In order to quantify the statistics of C, we employ a numerical Monte Carlo (MC) framework. A collection of realizations of the $Y(\boldsymbol{x})$ field are generated using a sequential Gaussian simulator (SGeMS; *Remy et al.*, 2009). The spatial covariance C_Y is modeled through a stationary Exponential model, characterized by isotropic correlation scale $\lambda = 8$ m and variance $\sigma_Y^2 = 3$. Consistent with previous studies (e.g., *de Barros et al.*, 2013; *Moslehi et al.*, 2015), a uniform generation grid, with elements of side $\Delta_x = \Delta_y = 1/8\lambda$, is employed. Transient groundwater flow and contaminant transport for each realization are respectively solved through the widely tested codes MODFLOW (*Harbaugh*, 2005) and MT3DMS (*Zheng and Wang*, 1999). A Lagrangian-Eulerian method, the Method of Characteristics (MOC), is applied to solve contaminant transport with MT3DMS. Further details pertaining the computational methods (and the associated numerical errors) adopted are documented in the literature (*Zheng* *and Bennet*, 2002). A comparison between the numerical methods utilized in this work with other existing codes can be found in *Hassan and Mohamed* (2003).

We explore three diverse pumping scenarios, indicated as scenarios I, II and III. Each scenario is characterized by a fixed total volume of water extracted (V_w) and a given operational scheme according to which the pumped flow rate is varied in time. Each of the transient scenarios is compared against a corresponding setting associated with steady-state pumping characterized by the same total volume of water extracted from the system during the simulated transient regime. Table 1 lists the main parameters used in the study. Note that the longitudinal Péclet number is set to 800. The Péclet number is given by $P_e = \lambda v_0 / D_x$, where $v_0 = q_0/\varphi$ denotes the imposed uniform-in-the-mean longitudinal velocity and D_x is the local scale longitudinal dispersion coefficient, which we set at the constant value listed in Table 1.

We perform MC numerical simulations of flow and contaminant transport according to the three scenarios displayed in Figure 2 (Figure 2a, b, and c respectively referring to scenarios I, II and III). The selected well pumping operation schedules are inspired by patterns employed in practical settings by groundwater management agencies to extract water from underground resources for diverse purposes (including, e.g., drinking and irrigation). As seen in Figure 2, scenario III is characterized by the highest variability of the dynamic pumping strategy.

Following a preliminary convergence study (not shown), we base our results on a set of 1000 MC simulations for each scenario and pumping strategy adopted. The results of the MC simulations are post-processed with the aim of capturing the temporal evolution of the mean and variance of the flux-averaged contaminant concentration recovered at the well. We note that the effects of variable well pumping operations on the solute breakthrough curve at the well can also depend on the ratio between the natural base flow Q_0 and the well pumping rate Q_w.

For each scenario we quantify the risk, defined here as the probability of failure, e.g., the probability that the contaminant concentration exceeds a given critical value at the well. According to this, we define risk (ξ) in this work in terms of exceeding probabilities (e.g., *de Barros and Fiori*, 2014):

$$\xi = P[C(\boldsymbol{x_w}, t) \geq C_{crit}], \tag{5}$$

where $C_{crit} \equiv C^*$, as introduced in Section 2, and P denotes probability. Note that the risk definition in Equation (5) rests on a full statistical distribution of the flux-averaged concentration at the pumping well as a function of time. As shown by several authors (*Kapoor and Kitanidis*, 1998; *Fiori and Dagan*, 2000, *de Barros and Fiori*, 2014), the mean concentration is insufficient to characterize risk and higher order moments are required. The mean concentration only becomes a meaningful measure of risk under ergodic conditions, i.e., large travel distances or large contaminant source dimensions with respect to the log-transmissivity correlation scale. If these conditions are satisfied, macrodispersion theory is expected to hold (*Dagan*, 1984; *Kitanidis*, 1988; Chapter 10 of *Rubin*, 2003 and references therein). In particular, *de Barros and Fiori* (2014) provides a detailed discussion on the need to use of a full probabilistic distribution to quantify risk by taking into account also the probability of extreme events (e.g., probability of concentration exceeding a very high or low value). The exceedance probability (5) is computed directly from the numerical MC results and informs decision makers on the probability that $C(\boldsymbol{x_w}, t) \geq C_{crit}$.

4. Results and Discussion

We start by illustrating the relevance of the problem tackled in this study through a discussion of some key differences between contaminant BTCs observed at the pumping well operating with a steady-state pumping strategy and a transient pumping scheme for selected exemplary realizations of the $Y(\boldsymbol{x})$ field. Second, we present the temporal evolution of the mean and variance (as well as the resulting coefficient of variation) of the flux-averaged concentration at the well for the pumping strategies of scenario III. The latter is representative of the main conclusions of our analysis, the results of scenarios I and II being fully documented in the Supplemental Material (SM). Third, we display the temporal behavior of risk, as defined in (5), for scenario III, under steady-state and transient pumping conditions. Corresponding outputs for scenarios I and II are included in the SM. Finally, we demonstrate the effects of local scale dispersion and aquifer heterogeneity on the uncertainty of the concentration BTCs for scenario III. We show how the interplay between pumping operations, aquifer heterogeneity and local scale dispersion affect the temporal patterns of the flux-averaged concentration uncertainty. The upcoming results also emphasize the importance of pumping in diluting the concentration at the well.

4.1. Concentration breakthrough curves observed at the pumping well for different pumping strategies

In this Section, we aim to provide a qualitative illustration of the way the concentration BTC at the well can be affected by the pumping operation and the heterogeneous transmissivity field. A graphical depiction of the effect of a time-dependent withdrawal schedule on the concentration BTC is provided in Figure 3. The latter depicts the concentration BTCs observed at the pumping well for three diverse realizations of $Y(\boldsymbol{x})$ under the constant and temporally varying pumping strategy of each scenario. Each plot within Figure 3 includes the contaminant BTCs resulting from a constant and a transient extraction strategy for a given realization of the $Y(\boldsymbol{x})$ field. Figures 3a, b, c refer to Scenario I, Figures 3d, e, f refer to Scenario II and finally, Figures 3g, h, i refer to Scenario III. The three distinct realizations of the transmissivity are denoted by T_1, T_2 and T_3 (see Figures SM17-SM19 of the SM) in Figure 3 and are selected solely for the purpose of illustration. These three realizations of the transmissivity fields (T_1, T_2 and T_3) were obtained through the software SGeMS (*Remy et al.*, 2009) and are characterized by the geostatistical parameters described in Section 3. As shown in Figure 3, significant differences are detected between the concentration BTCs obtained with uniform and variable in time pumping rates. From a qualitative standpoint, it can be noted that the concentration BTCs produced by a dynamic pumping regime are characterized by peaks of different strength and occurring at diverse times when compared to the corresponding BTCs obtained with uniform pumping. This result has strong implications in risk analysis, inasmuch as public health authorities are concerned with peak concentrations and the time of their occurrence (e.g., *de Barros and Rubin,* 2008; *Oladyshkin et al.,* 2012; *Siirila and Maxwell*, 2012). The results displayed in Figure 3 also illustrate the complex interaction between the hydrogeological heterogeneity of the aquifer and the transient flow regime induced by a temporally varying pumping schedule. These illustrative results point out the importance of considering temporally varying pumping settings, as employed in practical applications, when evaluating contaminant transport in a well field, with direct implication on risk caused by contamination of water extracted at the well.

4.2. Mean and variance of solute concentration at the pumping well

We compute and discuss here the temporal evolution of the first two statistical moments of the flux-averaged solute concentration detected at the pumping well. To streamline the presentation, we only show the results related to scenario III, which encapsulates the key observations of the analysis. Results associated with scenarios I and II are documented in the SM.

Figures 4 and 5 depict the mean and the variance of the flux-averaged concentration (respectively denoted as $\langle C \rangle$ and $Var[C]$) detected at the well following the adoption of a uniform (Figures 4a and 5a) and dynamic (Figures 4b and 5b) pumping strategy. These results indicate that the transient operational regime applied at the well has marked influence on the shape of the concentration BTCs. A striking observation is that the local minimum and maximum of the mean and variance of the flux-averaged concentration at the well occur at the same dimensionless time for both types of pumping regimes. This observed behavior is supported by theoretical developments illustrated in Appendix A.

Figure 4b shows that the mean flux-averaged concentration starts increasing when the plume approaches the well, until a maximum value is reached between dimensionless time values of 0.2 and 0.3. Figure 4b also reveals that an increase in the pumping rate can lead to a sudden decrease of the mean flux-averaged concentration. Due to the intermittent pumping schedule, this effect is seen to extend in time causing an oscillatory pattern of the mean BTC. It can be noted that activating the pumping well induces contaminant dilution at the well due to mixing of contaminated and clean water. This leads to a decrease of the contaminant concentrations in the water extracted at the well with respect to concentration levels in the contaminant plume (*Einarson and MacKay*, 2001, *de Barros et al.*, 2009).

A pronounced oscillatory pattern in time is detected for $Var[C]$ (Figure 5b). We note that an increase of the pumping rate corresponds to a decrease of $Var[C]$ across the various stress periods. This behavior is consistent with the observation that an increase of the extraction rate enhances the likelihood that the contaminant is captured by the well. This consequently tends to dampen the variability of contaminant concentrations observed at the well, with a corresponding reduction of $Var[C]$. The opposite tends to happen when the pumping rate is reduced (and eventually goes to zero), thus leading to increased values of $Var[C]$ at the well.

By comparing the variance of the flux-averaged concentration detected at the pumping well operating under a temporally variable strategy for the three investigated scenarios (Figure 5b addresses scenario III and Figures SM4 and SM8 of the SM respectively refer to scenarios I and II), we observe that the maximum values in Figure 5b (scenario III) are much higher than their counterparts appearing in Figure SM4 (scenario I) and Figure SM8 (scenario II) of the SM. We recall that scenario III is associated with the highest temporal variability of the well operational scheme. Our results indicate that the uncertainty associated with the flux-averaged concentration is higher for pumping strategy III than for pumping regimes I and II. This behavior is also supported by viewing the results of Figures 6 and 7, respectively depicting the coefficient of variation (*CV*) of the flux-averaged concentration for the constant and transient pumping strategy of scenario III and comparing them against the corresponding results depicted in the SM (see Figures SM9, SM10 for scenario I and Figures SM11 and SM12 for scenario II). When an extraction schedule with high temporal variability (see, e.g., scenario III) is applied at the well, the values of *CV* tend to increase, in particular during time intervals when pumping is stopped. We conclude that considering a high temporal variability of the pumping rate has the effect of increasing the uncertainty associated with the concentration observed at the pumping well. We observe that while it is well known that aquifer heterogeneity leads to uncertain contaminant transport prediction, our results indicate that the engineered operational pumping schedule, manifested through $Q_w(t)$, may play a major role in controlling the variability of the moments of flux-averaged concentration at the well. Results in Figures 6, 7, SM9, SM10, SM11, SM12 also show that uncertainty in the solute concentration at the well is large at both early and late times. This implies that the (ensemble) mean is not sufficient to characterize the transport behavior and quantification of higher order moments is needed.

4.3. Probability of exceedance of concentration limit value

We compute here the probability of failure, i.e. the probability that the contaminant concentration exceeds an established limit value, C^*. This probability represents a measure of risk, as defined in (5) and is computed on the basis of the MC realizations performed. The exceedance probability provided in Equation (5) enables one to evaluate the probability of extreme events since it contains information about the mean, variance and higher order moments of the flux-averaged concentration. Figures 8 and 9 depict the temporal evolution of $P(C > C^*)$ for the uniform and time-varying pumping strategies of scenario III. The choice of the operational scheme (constant or variable in time pumping) to withdraw a fixed water volume has a clear influence on the temporal evolution of risk (5) at the pumping well.

The results depicted in Figure 8 are linked to a temporal pattern which is similar to that of the mean flux-averaged concentration in Figure 4a. For the cases analyzed, the results suggest that higher mean concentration values are associated with increased probability to exceed the concentration threshold C^*. When considering transient pumping, we note that the mean contaminant concentration (Figure 4b) and the probability of exceedance (Figure 9) display similar patterns for the lowest values of the variance of the flux-averaged concentration observed at the pumping well (Figure 5b). This correspondence is not as evident for increased concentration variance (Figure 5b). As noted in Section 4.2, highly variable transient pumping strategies favor an increase of the uncertainty of solute concentrations at the pumping well. This, in turn, affects risk uncertainty, as quantified by (5). In general, we observe that the transient operational scheme selected in scenario III induces a temporal oscillating behavior of risk at the well (Figure 9), according to which risk tends to decrease with the temporal reduction of the mean concentration signal.

4.4. Local scale dispersion and hydrogeological heterogeneity

The previous sections considered a fixed level of heterogeneity and local scale dispersion (see list of parameters in Table 1). We now assess the impact of aquifer heterogeneity and local scale dispersion on the statistics of the flux-averaged concentration in the presence of variable pumping rates.

4.4.1. Impact of local scale dispersion on the concentration statistics

Figure 10 illustrates the influence of increasing local scale dispersion on the mean and on the variance of the flux-averaged concentration for the diverse pumping operations of Scenario III. The mean concentration for constant and variable pumping rates are shown in Figures 10a and 10b, respectively, whereas Figures 10c and 10d depict the concentration variance for constant and variable pumping schedules, respectively. The effect of local scale dispersion on the concentration variance is manifested through the longitudinal Péclet number, defined as $P_e = \lambda v_0 / D_x$. Figure 10 shows the results for both longitudinal $P_e = 800$ (corresponding to the parameters listed in Table 1) and $P_e = 200$ for a fixed level of heterogeneity (as rendered by σ_Y^2 = 3). The Péclet number of 200 corresponds to increased local scale dispersion (longitudinal and transverse dispersivities are set to 0.04 m and 0.0004 m, respectively). The remaining input parameters for the simulations related to $P_e = 200$ are the same as those reported in Table 1 of the manuscript.

As depicted in Figure 10, increasing the value of local scale dispersion (i.e., reducing P_e) leads to decreased values of the concentration variance (Figures 10c and 10d). This is related to the observation that dispersion smooths out the concentration gradients, hence reducing the sample-to-sample variability of transport observables at the well (e.g., *Kapoor and Kitanidis*, 1998; *Fiori and Dagan*, 2000; *Dentz and de Barros*, 2013). Note that the transient operational scheme applied at the well has marked influence on the concentration variance for both Péclet numbers considered, as opposed to what can be observed for the constant in time pumping scheme. This is mainly attributed to the following reasons. First, when the pumping rate is temporally variable, the solute plume residence time in the aquifer increases, thus allowing for the effects of local scale dispersion to become more pronounced. Second, temporally variable flows, induced by the action of dynamic pumping rates, tend to enhance solute spreading, which in turn augments dilution (see also *Dentz and Carrera*, 2003). Furthermore, this dilution enhancement (driven by the action of variable pumping rates) leads to an increase of the plume spatial extent (in the longitudinal and transverse directions) and to an increase in the probability of the plume being captured by the well, thus contributing to a reduction of the variance. For the set of parameters used in this numerical investigation, the significance of local scale dispersion on the reduction of the concentration variance is diminished for a constant pumping rate (compare Figure 10c and 10d). It is important to note that the joint effects of local scale dispersion and pumping operations on the concentration variance will also depend on the distance between the contaminant source and the receptor (i.e., the pumping well). With reference to the effect of local scale dispersion on the concentration mean at the extracting well (Figures 10a and 10b), we notice that the differences between the two values of P_e considered are smaller as compared to the corresponding differences detected in the temporal evolution of the concentration variance displayed in Figures 10c and 10d. When we increase local scale dispersion, the mean concentration does not change much for a constant pumping schedule (Figure 10a) because the distance between the source and the operating well is not sufficiently large in our scenario (approximately equal to 10 λ). Therefore, the effects of local scale dispersion are not that evident on the temporal evolution of the mean concentration. We recall that the advective time scale is the same for both values of P_e. On the other hand, for the case of transient pumping (Figure 10b), the residence time of the plume in the aquifer increases, thus allowing for the effects of P_e to become slightly visible. A further increase of the travel distance of the contaminated plume will enhance the effects of local scale dispersion on the mean concentration for both pumping operations (constant and variable in time).

4.4.2. Impact of aquifer heterogeneity on the concentration statistics

In the following, we investigate the sensitivity of the concentration statistics to the degree of aquifer heterogeneity in the presence of both constant and time-varying pumping schedule. The level of aquifer heterogeneity is epitomized by the log-conductivity variance σ_Y^2.

Figure 11 provides a comparison between the mean (Figures 11a and 11b) and variance (Figures 11c and 11d) of the flux-averaged concentration at the well for σ_Y^2 = 0.5 and 3 under a constant and temporally dynamic pumping operations. The larger log-transmissivity variance ($\sigma_Y^2 = 3$) yields an increased likelihood of the occurrence of preferential flow paths within the aquifer which contribute to faster solute arrival. Solute migration through these high velocity paths tends to be locally dominated by advection and the solute reaches the pumping well at earlier times (Figures 11a and 11b). The temporal evolution of the mean concentration displayed in Figures 11a and 11b for both log-transmissivity variances also shows that an increased strength of σ_Y^2 can also augment the probability of occurrence of low conductivity zones that can entrap solute, resulting in late arrival times. This contrast between low and high transmissivity values for larger σ_Y^2 causes the plume to spread erratically and facilitates the exchange of solute mass between streamtubes (i.e., dilution enhancement). In order words, higher permeability variability tends to reduce the mean solute concentration and smooths out concentration gradients, thus reducing concentration variance (Figures 11c and 11d). The numerical results in Figures 11c and 11d illustrate that the differences between the concentration variance obtained for $\sigma_Y^2 = 0.5$ and 3 are higher when the pumping operation varies in time. The dynamic pumping scheme also increases the magnitude of the concentration mean and variance when σ_Y^2 is lower (Figures 11b and 11d).

We remind that the results displayed in Figure 11 are not completely general because other factors can play a role in the uncertainty of the concentration statistics. These additional factors include the solute travel distance, source release conditions, location of the solute source, the conceptualization of the heterogeneity model and the presence of chemical reactions. Nevertheless, it is evident that the interplay between aquifer heterogeneity and pumping operation plays fundamental role in probabilistic risk assessment. Figure 12 shows the temporal variability of the risk (probability of exceedance), defined in Equation (5), for constant and dynamic pumping operations and different values of σ_Y^2. With the exception of the early and late time regimes, the results in Figure 12 show that the probability of observing a concentration value larger than a critical value is higher for low than for high heterogeneity. The reason for this behavior is similar to the discussion related to Figure 11c and 11d; i.e., larger values of σ_Y^2 facilitate mass transfer between neighboring streamtubes, a phenomenon which enhances dilution and, as a consequence, results in a larger probability of having lower concentration values. Therefore, the effects of the interplay between advection and local-scale dispersion become more evident for larger σ_Y^2, resulting in a tendency to lower the risks at the operating well (see Figure 12 for both pumping schemes). Otherwise, larger heterogeneity leads to higher risks at the early and late times. We highlight that the risk computed for an aquifer with high heterogeneity persists for longer periods of times (compare results obtained for $\sigma_Y^2 = 0.5$ and $\sigma_Y^2 = 3$). This is a consequence of the increased tailing effects of the concentration BTC observed in each MC realization when heterogeneity is large. For the numerical set-up adopted in this work, we show that the pumping operation scheme has a significant controlling role on the temporal evolution of the risk. As depicted in Figure 12b, the temporal variability of the risk and its multiple peaks are controlled by the temporal patterns of the pumping rate.

Albeit the focus of the current work lies on the interplay between aquifer heterogeneity and pumping operation (i.e., engineering factors) on the uncertainty of the concentration BTC, we include results in the SM for a homogeneous aquifer (i.e., constant transmissivity field). Figure SM21 shows how the pumping operation can affect the asymmetry of the concentration

BTC under uniform flow fields. Furthermore, as shown in Figures SM20 and SM21, the peak concentration in the deterministic homogeneous scenario is higher for both pumping operations when compared to the heterogeneous aquifers. Figure 13 depicts the temporal evolution of the concentration mean for different values of aquifer heterogeneity (σ_Y^2 = 0.5, $\sigma_Y^2 = 3$ and for the homogeneous case). The increase of the mean concentration with lower heterogeneity is linked to the selected location of the solute source zone (recall that, in the settings we analyze, the centroid of the source zone is aligned with the location of the well). Plume meandering is less pronounced for lower heterogeneous aquifers (when compared to higher heterogeneity in Y), therefore the probability of the plume being captured by the well is higher for low values of σ_Y^2 in our settings. Figures SM20 and SM21 depict the suite of results for the case of a deterministically homogeneous aquifer ($\sigma_Y^2 = 0$).

5. Conclusions

We study and compare the effect of temporally variable and uniform pumping regimes on key features of contaminant transport in a randomly heterogeneous aquifer. Our work considers the joint effects of spatially heterogeneous hydraulic conductivity (or transmissivity) and temporally varying well pumping rates and offers some insights on a realistic approach for the evaluation of the risk associated with contamination of groundwater extracted at the pumping well location. The analysis is performed within a stochastic framework upon relying on the numerical study of three distinct pumping scenarios.

The two leading statistical moments of the flux-averaged contaminant concentrations recovered at the well are computed. We document the way the temporally dynamic pumping rate augments the uncertainty in the flux-averaged concentration at the well. We then provide an appraisal of risk at the well by computing the probability that the contaminant concentration exceeds a defined threshold value (i.e., probability of failure).

Our work leads to the following major conclusions.

1. In addition to aquifer heterogeneity, the use of a transient pumping strategy at the well can markedly affect the temporal evolution of contaminant concentration BTCs and statistical moments. We show that dynamic pumping strategies induce multiple peaks in the mean and variance of the flux-averaged concentration detected at the extraction well.
2. Lowest and largest values of mean and variance of flux-averaged concentration at the well tend to occur at the same time. This observation is supported by our numerical findings and by analytical results illustrated in Appendix A.
3. The activation of the pumping well (or the increase of its extraction rate) induces contaminant dilution with fresh water at the well. As a consequence, the detected contaminant concentration tends to be reduced.
4. The choice of the type of engineering control to the temporal sequence of well pumping rates could represent a key factor in quantifying the uncertainty of the contaminant concentration detected at the well. This observation is supported by considering that uncertainty associated with detected BTCs at the well increases for highly variable pumping regimes (compare scenario III against scenarios I and II). We show that this controlling role of the temporal extraction schedule on uncertainty has direct consequences to risk analysis. The selection of a dynamic pumping regime has a clear influence on the temporal evolution of risk, as defined in (5), at the well, i.e., pumping rate fluctuations induce a temporally oscillating risk pattern. The mean flux-averaged solute concentration and the probability of exceedance of a given threshold value show a similar temporal

evolution when the variance of flux-averaged concentrations at the pumping well is small. In these cases, larger mean concentration values correspond to larger probability of exceedance of a given concentration threshold. Otherwise, this correspondence was not detected in our cases for increased concentration variance.

Our findings suggest that risk analysis should incorporate dynamic pumping rates to reflect realistic operational practices and be able to provide important information to risk managers, including realistic quantifications of the uncertainty associated with risk at the pumping well.

Note that the results and conclusions presented in this study are confined to a hydrogeological setting whose randomly heterogeneous conductivity is characterized by given sets of parameters. The results can be impacted by other factors, including, e.g., the distance between the contaminant source and the receptor, the dimensions of the source zone, mass release conditions, the ratio of the base flow discharge with respect to the pumping rate, chemical reactions and the conceptualization of the hydrogeological heterogeneity. The influence of variable pumping rates on probabilistic risk analysis depends on the interactions between temporal fluctuations induced by the action of pumping, local scale dispersion, and spatial heterogeneity. Quantifying the effects of the overall spectrum of scenarios is complex due to the interplay of three distinct time scales defined by the pumping well operation, advection and local scale dispersion. The relative importance of the temporally variable pumping rate on risk will depend on the ratio between these characteristic time scales and should be subject of further investigation. As a future projection of the study, one can incorporate in our methodological framework adverse human health effects (e.g., *Andričević and Cvetković*, 1996, *de Barros and Rubin*, 2008) and other well vulnerability criteria, including, e.g., the time taken to breach a certain quality objective (e.g., drinking standard) at the well, the total time of well failure (i.e., non-compliance with a quality objective), and the time taken to recover the well from failure.

Appendix A: Low-order moments of the flux-averaged concentration

This appendix provides theoretical developments supporting the observed correspondence between the low and high values in the mean and variance of the flux-averaged concentration (see Figures 4-5). We start by considering the migration of a solute plume originating far from the operating pumping well from a source zone of volume V_0 located upstream of the well. To simplify the derivation, we quantify the mean and variance of mass flux at a control plane located far away from the well and spanning the wellhead protection area (WHPA) along a direction normal to the mean background groundwater flow (see Figure A.1). Under this setting, we assume that the pumping rate at the well is constant such that $Q_w(t) = Q_w$ and develop theoretical expressions for the moments of flux-averaged concentrations under a uniform-in-the-mean flow condition. As such, the key purpose of our subsequent developments is to establish an analogy with the observations stemming from the numerical results illustrated in Section 4. We obtain an approximation for the mean and variance of the flux-averaged concentration at the control plane by making use of the Lagrangian framework developed by *Dagan et al.* (1992). For further details on the Lagrangian approach, the reader is referred to Chapters 9 and 10 of *Rubin* (2003). Given the purpose of the analogy, we neglect the effects of local-scale dispersion (e.g., transport is purely advective) in the following derivations and discussion.

We start by defining $C(t)$ as the flux-averaged contaminant concentration [M/L^3] measured at the control plane described above (denoted by CP)

$$C(t) = \frac{Q_m(t)}{Q_w}. \tag{A.1}$$

We respectively denote $Q_m(t)$ [M/T] and Q_w [L^3/T] as the solute mass and volumetric flow rate across the CP at time *t*. Since Q_w is deterministic in our work, the statistics of $C(t)$ depend only on the statistics of $Q_m(t)$. For initial concentration c_o instantaneously and uniformly injected within a volume V_0, the mean of $Q_m(t)$ can be expressed as:

$$\langle Q_m(t|\tilde{\boldsymbol{a}})\rangle = C_0 \int_{V_0} g_1(t|\tilde{\boldsymbol{a}})d\tilde{\boldsymbol{a}}. \tag{A.2}$$

with $\tilde{\boldsymbol{a}}$ indicating the initial location (within V_0) of a solute particle released in the aquifer, $g_1(t|\tilde{\boldsymbol{a}})$ being the solute travel time probability density function (PDF) from the source to the CP. The second moment of $Q_m(t)$ can be expressed as:

$$\langle [Q_m(t|\tilde{\boldsymbol{a}})]^2\rangle = {C_0}^2 \int_{V_0}\int_{V_0} g_2(t,t|\tilde{\boldsymbol{a}}',\tilde{\boldsymbol{a}}'')d\tilde{\boldsymbol{a}}'d\tilde{\boldsymbol{a}}'', \tag{A.3}$$

where $g_2(t,t|\widetilde{\boldsymbol{a}}',\widetilde{\boldsymbol{a}}'')$ is the two-particle travel time PDF. The variance of $Q_m(t)$ is obtained by evaluating $Var[Q_m] = \langle [Q_m]^2 \rangle - \langle Q_m \rangle^2$. For low heterogeneity, e.g. $\sigma_Y^2 < 1$, the PDF g_1 can be represented by a lognormal distribution (*Dagan et al.*, 1992; *Cvetkovic et al*., 1992; *Selroos and Cvetkovic*, 1994). This result has been verified numerically (*Rubin*, 2003; *Gotovac et al.*, 2009). Under this assumption, g_1 scales as:

$$g_1(t) \sim \frac{1}{t} e^{-(lnt)^2}. \tag{A.4}$$

By the same token, the two-particle travel time PDF g_2 scales as:

$$g_2(t) \sim \frac{1}{t^2} e^{-(lnt)^2}. \tag{A.5}$$

We observe that $\sqrt{g_2}$ evolves like g_1. Thus, the temporal evolution of the mean and variance of $Q_m(t)$ (and consequently of $C(t)$) are similar (see (A.2) and (A.3)). This theoretical finding, albeit under the simplified conditions here considered, constitutes an additional support to the temporal coincidence between maxima and minima of the mean and the variance of $C(t)$ observed in our work. Note that the travel time scaling we derive is strictly valid for low values of log-conductivity/transmissivity variance. It can nevertheless serve as an approximation for moderate to high variances as seen for example in the work of *Salandin and Fiorotto* (1998) who found a good quality agreement between longitudinal velocity covariances obtained through numerical Monte Carlo simulations and first-order theory for log-conductivity variance as large as 4 under uniform-in-the-mean flow.

Acknowledgments

The first author gratefully acknowledges the financial support provided by Foundation for Cross-Connection Control and Hydraulic Research at the University of Southern California. Funding from the EU and MIUR (Italian ministry of Education, University and Research) under the Water JPI, WaterWorks 2014 framework (project: WE-NEED- Water NEEDs, availability, quality and sustainability) is also acknowledged. We are grateful to Mariaines Di Dato for the editorial assistance. The authors also thank the Editor, the Associate Editor and two anonymous Reviewers for their constructive comments.

References

Andričević, R., Cvetković, V., 1996. Evaluation of Risk from Contaminants Migrating by Groundwater. Water Resour. Res. 32 (3), 611-621.

Assouline, S., Möller, M., Cohen, S., Ben-Hur, M., Grava, A., Narkis, K., Silber, A., 2006. Soil-plant system response to pulsed drip irrigation and salinity. Soil Sci. Soc. Am. J. 70 (5), 1556-1568.

Bear, J., Jacobs, M., 1965. On the movement of water bodies injected into aquifers. J. Hydrol. 3 (1), 37-57.

Chang, L. C., Shoemaker, C. A., Liu, P. L. F., 1992. Optimal time-varying pumping rates for groundwater remediation: Application of a constrained optimal control algorithm. Water Resour. Res. 28 (12), 3157-3173.

Chen, Y., Lu, C., Luo, J., 2012. Solute transport in divergent radial flow with multistep pumping. Water Resour. Res. 48, W02510, doi:10.1029/2011WR010692.

Cole, B., Silliman, S., 1997. Capture zones for passive wells in heterogeneous unconfined aquifers. Ground Water 35 (1), 92-98.

Cvetkovic, V., Shapiro, A. M., Dagan, G., 1992. A solute flux approach to transport in heterogeneous formations: 2. Uncertainty analysis. Water Resour. Res. 28 (5), 1377-1388, doi:10.1029/91WR03085.

Dagan, G., 1982. Stochastic modeling of groundwater flow by unconditional and conditional probabilities: 1. Conditional simulation and the direct problem. Water Resour. Res. 18(4), 813-833.

Dagan, G., 1984. Solute transport in heterogeneous porous formations. J. Fluid Mech. 145, pp. 151–177. doi:10.1017/S0022112084002858.

Dagan, G., Cvetkovic, V., Shapiro, A., 1992. A solute flux approach to transport in heterogeneous formations: 1. The general framework. Water Resour. Res. 28 (5), 1369–1376, doi:10.1029/91WR03086.

Dagan, G., Neuman, S. P., 1997. Subsurface flow and transport: a stochastic approach. Cambridge University Press.

de Barros, F. P. J., Fiori, A., 2014. First-order based cumulative distribution function for solute concentration in heterogeneous aquifers: Theoretical analysis and implications for human health risk assessment. Water Resour. Res. 50 (5), 4018-4037.

de Barros, F. P. J., Guadagnini, A., Fernàndez-Garcia, D., Riva, M., Sanchez-Vila, X., 2013. Controlling scaling metrics for improved characterization of well-head protection regions. J. Hydrol. 494, 107-115.

de Barros, F. P. J., Rubin, Y., 2008. A risk-driven approach for subsurface site characterization. Water Resour. Res. 44, W01414, doi:10.1029/2007WR006081.

de Barros, F. P. J., Rubin, Y. and Maxwell, R. M., 2009. The concept of comparative information yield curves and its application to risk-based site characterization. Water Resour. Res. 45, W06401, doi:10.1029/2008WR007324.

Dentz, M., Carrera, J., 2003. Effective dispersion in temporally fluctuating flow through a heterogeneous medium. Phys. Rev. E 68. doi:10.1103/ PhysRevE.68.036310.

Dentz M., de Barros F. P. J., 2013. Dispersion variance for transport in heterogeneous porous media. Water Resour. Res. 49(6):3443–61. http://dx.doi.org/10. 1002/wrcr.20288.

Einarson, M. D., Mackay, D. M., 2001. Peer Reviewed: Predicting Impacts of Groundwater Contamination. Environ. Sci. Technol. 35 (3), 66A-73A.

Enzenhoefer, R., Nowak, W., Helmig, R., 2012. Probabilistic exposure risk assessment with advective–dispersive well vulnerability criteria. Adv. Water Resour. 36, 121-132.

Feyen, L., Beven, K. J., De Smedt, F., Freer, J., 2001. Stochastic capture zone delineation within the generalized likelihood uncertainty estimation methodology: conditioning on head observations. Water Resour. Res. 37 (3), 625-638.

Festger, A. D., Walter, G. R., 2002. The Capture Efficiency Map: The Capture Zone Under Time-Varying Flow. Ground Water 40 (6), 619-628.

Fiori, A., Dagan, G., 2000. Concentration fluctuations in aquifer transport: A rigorous first-order solution and applications. J. Contam. Hydrol. 45(1), 139-163.

Franzetti, S., Guadagnini, A., 1996. Probabilistic estimation of well catchments in heterogeneous aquifers. J. Hydrol. 174 (1), 149-171.

Frind, E. O., Molson, J. W., Rudolph, D. L., 2006. Well vulnerability: a quantitative approach for source water protection. Ground Water 44 (5), 732-742.

Gelhar, L. W., 1993. Stochastic subsurface hydrology. Prentice-Hall.

Gotovac, H., Cvetkovic, V., Andricevic, R., 2009. Flow and travel time statistics in highly heterogeneous porous media. Water Resour. Res. 45, W07402, doi:10.1029/2008WR007168.

Guadagnini, A., Franzetti, S., 1999. Time-related capture zones for contaminants in randomly heterogeneous formations. Ground Water 37 (2), 253-260.

Harbaugh, A. W., 2005. MODFLOW-2005, the US Geological Survey modular ground-water model: the ground-water flow process (pp. 6-A16). Reston, VA, USA: US Department of the Interior, US Geological Survey.

Hashimoto, T., Stedinger, J. R., Loucks, D. P., 1982. Reliability, resiliency, and vulnerability criteria for water resource system performance evaluation. Water Resour. Res. 18(1), 14-20.

Hassan, A. E., and Mohamed, M. M., 2003. On using particle tracking methods to simulate transport in single-continuum and dual continua porous media. J. Hydrol., 275(3), 242-260.

Indelman, P., Dagan, G., 1999. Solute transport in divergent radial flow through heterogeneous porous media. J. Fluid Mech. 384, 159-182.

Jacobson, E., Andricevic, R., Morrice, J., 2002. Probabilistic capture zone delineation based on an analytic solution. Ground Water 40 (1), 85-95.

Kapoor, V., Kitanidis, P. K., 1998. Concentration fluctuations and dilution in aquifers. Water Resour. Res. 34(5), 1181-1193.

Kitanidis, P. K., 1988. Prediction by the Method of Moments of Transport in a Heterogeneous Formation. J. Hydrol. 102 (1-4), 453-473.

Kreft, A., Zuber, A., 1979. On the use of the dispersion model of fluid flow. Int. J. Appl. Radiat. Is. 30 (11), 705-708.

Leray, S., de Dreuzy, J. R., Aquilina, L., Vergnaud-Ayraud, V., Labasque, T., Bour, O., Le Borgne, T., 2014. Temporal evolution of age data under transient pumping conditions. J. Hydrol. 511, 555-566.

Lu, Z., Zhang, D., 2003. On stochastic study of well capture zones in bounded, randomly heterogeneous media. Water Resour. Res. 39 (4), 1100, doi:10.1029/2002WR001633.

Molson, J. W., Frind, E. O., 2012. On the use of mean groundwater age, life expectancy and capture probability for defining aquifer vulnerability and time-of-travel zones for source water protection. J. Contam. Hydrol. 127 (1), 76-87.

Moslehi, M., Rajagopal, R., de Barros, F. P. J., 2015. Optimal allocation of computational resources in hydrogeological models under uncertainty. Adv. Water Resour. 83, 299-309.

Neupauer, R. M., Meiss, J. D., Mays, D. C., 2014. Chaotic advection and reaction during engineered injection and extraction in heterogeneous porous media. Water Resour. Res. 50 (2), 1433-1447.

Oladyshkin, S., de Barros, F. P. J., Nowak, W., 2012. Global sensitivity analysis: a flexible and efficient framework with an example from stochastic hydrogeology. Adv. Water Resour. 37, 10-22.

Pedretti, D., Fiori, A., 2013. Travel time distributions under convergent radial flow in heterogeneous formations: Insight from the analytical solution of a stratified model. Adv. Water Resour. 60, 100-109.

Ramanarayanan, T. S., Storm, D. E., Smolen, M. D., 1995. Seasonal pumping variation effects on wellhead protection area delineation. Water Resour. Bull. 31, No. 3: 421–430.

Reilly, T. E., & Pollock, D. W., 1996. Sources of water to wells for transient cyclic systems. Ground Water 34 (6), 979-988.

Remy, N., Boucher, A., Wu, J., 2009. Applied geostatistics with SGeMS: A user's guide. Cambridge University Press.

Riva, M., Guadagnini, A., De Simoni, M., 2006. Assessment of uncertainty associated with the estimation of well catchments by moment equations. Adv. Water Resour. 29 (5), 676-691.

Riva, M., Guadagnini, A., Ballio, F., 1999. Time-related capture zones for radial flow in two dimensional randomly heterogeneous media. Stoch. Env. Res. Risk A. 13 (3), 217-230.

Rubin, Y., 1991. Transport in heterogeneous porous media: Prediction and uncertainty. Water Resour. Res. 27(7), 1723-1738.

Rubin, Y., 2003. Applied Stochastic Hydrogeology. Oxford University Press, Oxford.

Salandin, P., Fiorotto, V., 1998. Solute transport in highly heterogeneous aquifers. Water Resour. Res. 34(5), 949-961.

Selroos, J.-O., Cvetkovic, V., 1994. Mass flux statistics of kinetically sorbing solute in heterogeneous aquifers: Analytical solution and comparison with simulations. Water Resour. Res. 30 (1), 63–69, doi:10.1029/93WR02654.

Siirila, E. R., Maxwell, R. M., 2012. A new perspective on human health risk assessment: Development of a time dependent methodology and the effect of varying exposure durations. Sci. Total Environ., 431, 221-232.

Stauffer, F., Attinger, S., Zimmermann, S., Kinzelbach, W., 2002. Uncertainty estimation of well catchments in heterogeneous aquifers. Water Resour. Res. 38 (11), 1238, doi:10.1029/2001WR000819.

van Leeuwen, M., te Stroet, C., Butler, A. P., Tompkins, J. A., 1998. Stochastic determination of well capture zones. Water Resour. Res. 34 (9), 2215-2223.

van Leeuwen, M., Butler, A., te Stroet, C., Tompkins, J., 2000. Stochastic determination of well capture zones conditioned on regular grids of transmissivity measurements. Water Resour. Res. 36 (4), 949–957.

Varljen, M. D., Shafer, J. M., 1991. Assessment of Uncertainty in Time-Related Capture Zones Using Conditional Simulation of Hydraulic Conductivity. Ground Water, 29 (5), 737-748.

Vassolo, S., Kinzelbach, W., Schäfer, W., 1998. Determination of a well head protection zone by stochastic inverse modelling. J. Hydrol. 206 (3), 268–280.

Vesselinov, V. V., 2007. Uncertainties in Transient Capture-Zone Estimates of Groundwater Supply Wells. J. Contemp. Water Res. Educ. 137 (1), 1-7.

Zheng, C., Wang, P. P., 1999. MT3DMS: a modular three-dimensional multispecies transport model for simulation of advection, dispersion, and chemical reactions of contaminants in groundwater systems; documentation and user's guide. Alabama Univ University.

Zheng, C., Bennet, G.D., 2002, Applied Contaminant Transport Modeling, Second Edition, Wiley Inter-Science, New York.

Tables

(L_x, L_y)	Flow Domain	(170 m,150 m)
(Δ_x, Δ_y)	Grid size	1/8 λ m, 1/8 λ m
λ	Correlation length of *Y*	8 m
σ_Y^2	Variance of *Y*	3
φ	Porosity	0.2
J	Mean head gradient	0.005882
T	Average Transmissivity	1 m^2/d
D_x	Longitudinal dispersion coefficient	2.94 x 10^{-4} m^2/d
D_y	Transverse dispersion coefficient	2.94 x 10^{-6} m^2/d
(x_w, y_w)	Location of the pumping well	(114.5 m, 74.5 m)
Q_w	Temporal sequence of pumping rate for scenario I	0.6 (uniform pumping rate) vs 0.8/0.4/0.8/0.4/0.8/0.4/0.8/0.4/0.8/0.4/0.8/0.4/0.8/0.4/0.8/0.4 m^3/d
Q_w	Temporal sequence of pumping rate for scenario II	0.45 (uniform pumping rate) vs 0.8/0.7/0.6/0.5/0.4/0.3/0.2/0.1/0.8/0.7/0.6/0.5/0.4/0.3/0.2/0.1 m^3/d
Q_w	Temporal sequence of pumping rate for scenario III	0.3 (uniform pumping rate) vs 0.8/0/0.4/0/0.8/0/0.4/0/0.8/0/0.4/0/0.8/0/0.4/0 m^3/d
q_o	Groundwater specific discharge	5.882 x 10^{-3} m/d
V_w	Volume of extracted water for scenario I	2880 m^3
V_w	Volume of extracted water for scenario II	2160 m^3
V_w	Volume of extracted water for scenario III	1440 m^3
C^*	Contaminant concentration threshold	10 g/m^3

Table 1. Parameter set employed in the numerical simulations.

Figure Captions

Fig. 1. Schematic representation of the problem studied. A two-dimensional flow field characterized by the presence of a pumping well and a uniform (in the mean) base flow from left to right of the domain is considered. The contaminant source is rectangular with longitudinal dimension L_1 and transverse dimension L_2, located at distance L from the well positioned at $\boldsymbol{x_w} = (x_w, y_w)$. The contaminant source is aligned with respect to the pumping well center.

Fig. 2. Pumping scenarios analyzed in the study: Scenario (a) I; (b) II; (c) III.

Fig. 3. Contaminant concentration BTCs observed at the pumping well for the three scenarios analyzed: Scenario I (plots a, b, c); Scenario II (plots d, e, f); and Scenario III (plots g, h, i).

Fig. 4. Mean concentration $\langle C \rangle$ observed at the pumping well for the uniform pumping strategy of Scenario III (a) and the transient pumping strategy of Scenario III (b).

Fig. 5. Variance of the concentration $Var[C]$ observed at the pumping well for the uniform pumping strategy of Scenario III (a) and the transient pumping strategy of Scenario III (b).

Fig. 6. Coefficient of variation *CV* of the concentration observed at the pumping well for the uniform pumping strategy of Scenario III.

Fig. 7. Coefficient of variation *CV* of the concentration observed at the pumping well for the transient pumping strategy of Scenario III.

Fig. 8. Sample probability of exceedance of the concentration threshold $P(C > C^*)$ for the uniform pumping strategy of Scenario III.

Fig. 9. Sample probability of exceedance of the concentration threshold $P(C > C^*)$ for the transient pumping strategy of Scenario III.

Fig. 10. Impact of the Péclet number (P_e) on the concentration mean for (a) constant and (b) time-varying pumping rate. Impact of the Péclet number (P_e) on the concentration variance for (c) constant and (d) time-varying pumping rate. Purple curves refer to P_e = 800 and blue curves refer to P_e = 200.

Fig. 11. Mean concentration for (a) constant and (b) time-varying pumping rates. Variance behavior is also depicted for (c) constant and (d) time-varying pumping schemes. Blue curves refer to low heterogeneity and purple curves to high heterogeneity.

Fig. 12. Probability of exceedance of the concentration threshold $P(C > C^*)$ for (a) constant and (b) time-varying pumping rates. Blue curves refer to low heterogeneity and purple curves to high heterogeneity.

Fig. 13. Mean concentration $\langle C \rangle$ observed at the pumping well for (a) constant and (b) time-varying pumping strategy of Scenario III for different levels of aquifer heterogeneity.

Fig. A.1. Schematic representation of the problem analyzed using the Lagrangian framework.

Figures and Captions

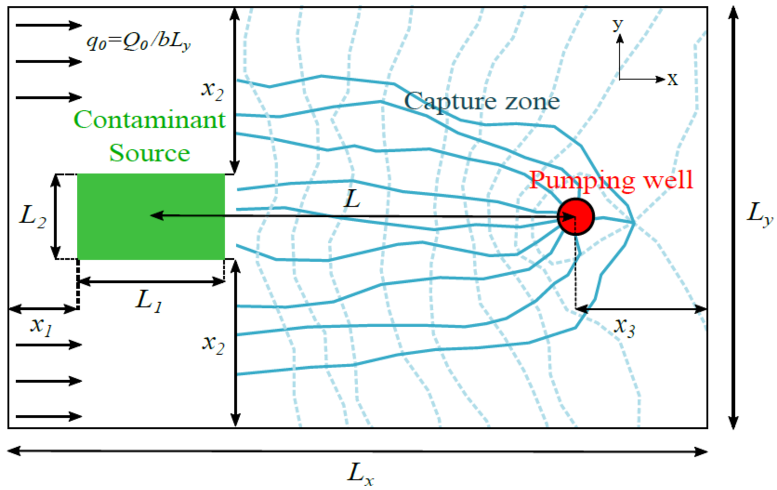

Fig. 1. Schematic representation of the problem studied. A two-dimensional flow field characterized by the presence of a pumping well and a uniform (in the mean) base flow from left to right of the domain is considered. The contaminant source is rectangular with longitudinal dimension L_1 and transverse dimension L_2, located at distance L from the well positioned at $\boldsymbol{x_w} = (x_w, y_w)$. The contaminant source is aligned with respect to the pumping well center.

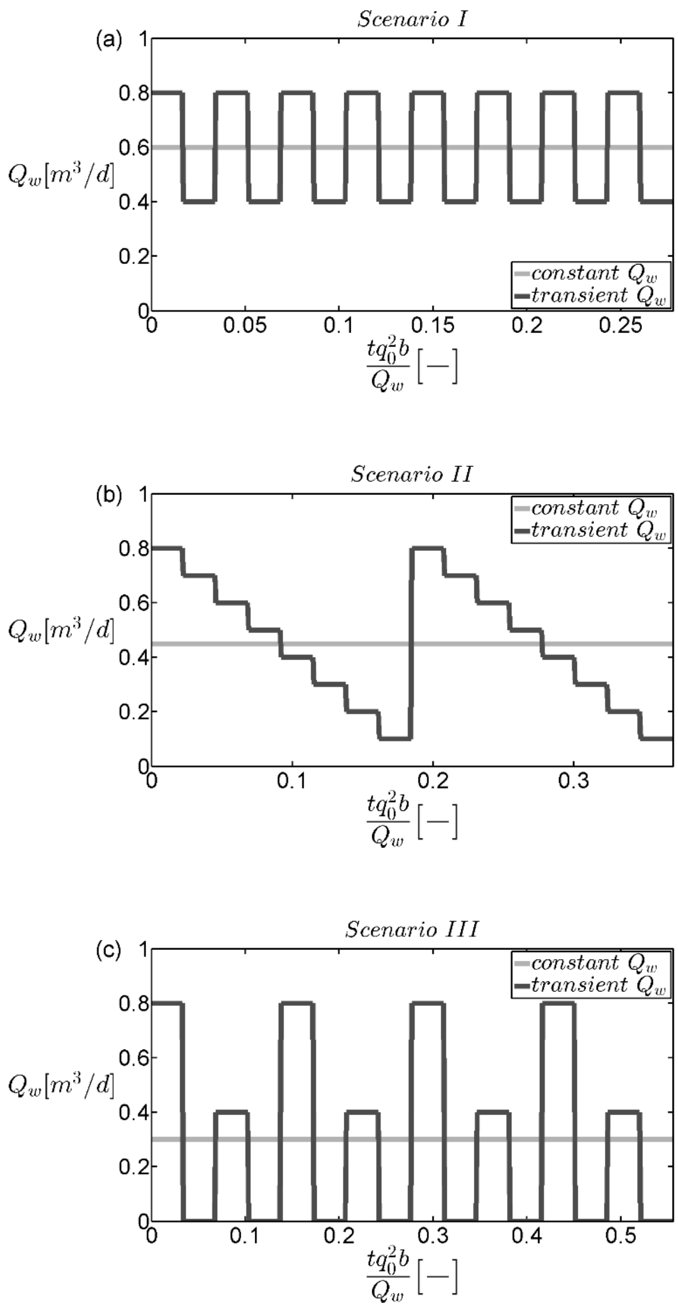

Fig. 2. Pumping scenarios analyzed in the study: Scenario (a) I; (b) II; (c) III.

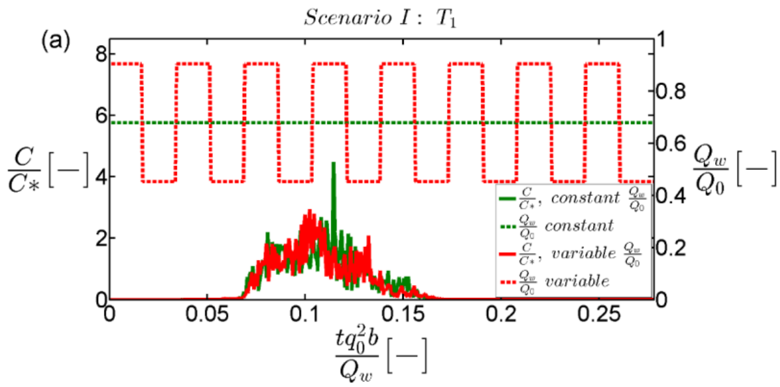

$Scenario\ I:\ T_1$
(a)
$\frac{C}{C*}[-]$
$\frac{Q_w}{Q_0}[-]$
$\frac{tq_0^2b}{Q_w}[-]$
$\frac{C}{C*}$, constant $\frac{Q_w}{Q_0}$
$\frac{Q_w}{Q_0}$ constant
$\frac{C}{C*}$, variable $\frac{Q_w}{Q_0}$
$\frac{Q_w}{Q_0}$ variable

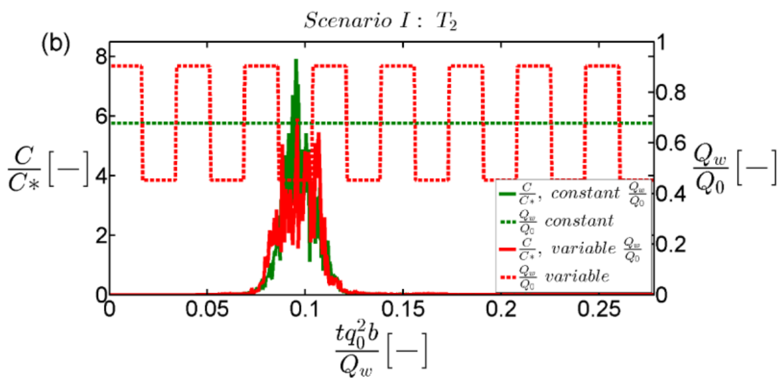

$Scenario\ I:\ T_2$
(b)
$\frac{C}{C*}[-]$
$\frac{Q_w}{Q_0}[-]$
$\frac{tq_0^2b}{Q_w}[-]$
$\frac{C}{C*}$, constant $\frac{Q_w}{Q_0}$
$\frac{Q_w}{Q_0}$ constant
$\frac{C}{C*}$, variable $\frac{Q_w}{Q_0}$
$\frac{Q_w}{Q_0}$ variable

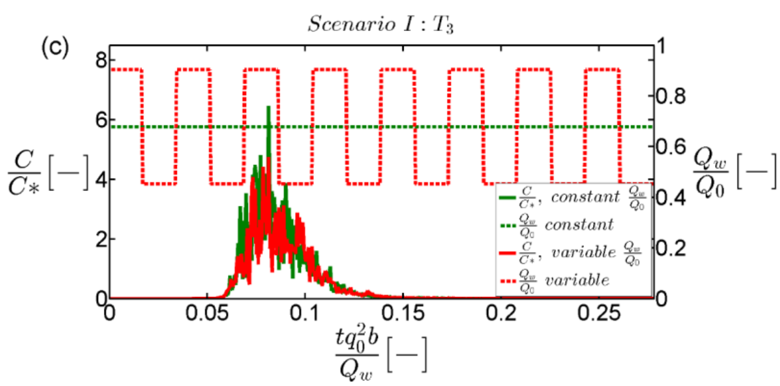

$Scenario\ I: T_3$
(c)
$\frac{C}{C*}[-]$
$\frac{Q_w}{Q_0}[-]$
$\frac{tq_0^2b}{Q_w}[-]$
$\frac{C}{C*}$, constant $\frac{Q_w}{Q_0}$
$\frac{Q_w}{Q_0}$ constant
$\frac{C}{C*}$, variable $\frac{Q_w}{Q_0}$
$\frac{Q_w}{Q_0}$ variable

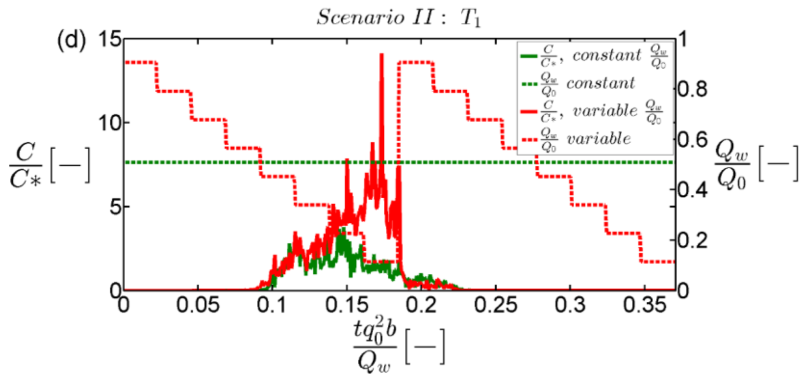
$Scenario\ II:\ T_1$
(d)
$\frac{C}{C*}[-]$
$\frac{Q_w}{Q_0}[-]$
$\frac{tq_0^2b}{Q_w}[-]$
$\frac{C}{C*}$, constant $\frac{Q_w}{Q_0}$
$\frac{Q_w}{Q_0}$ constant
$\frac{C}{C*}$, variable $\frac{Q_w}{Q_0}$
$\frac{Q_w}{Q_0}$ variable
0 5 10 15
0 0.2 0.4 0.6 0.8 1
0 0.05 0.1 0.15 0.2 0.25 0.3 0.35

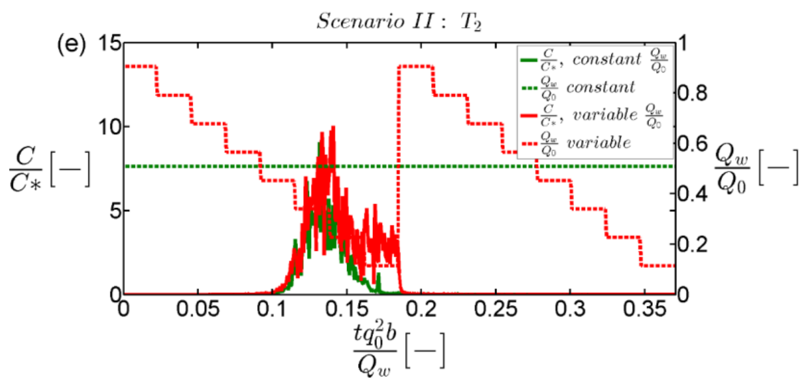
$Scenario\ II:\ T_2$
(e)
$\frac{C}{C*}[-]$
$\frac{Q_w}{Q_0}[-]$
$\frac{tq_0^2b}{Q_w}[-]$
$\frac{C}{C*}$, constant $\frac{Q_w}{Q_0}$
$\frac{Q_w}{Q_0}$ constant
$\frac{C}{C*}$, variable $\frac{Q_w}{Q_0}$
$\frac{Q_w}{Q_0}$ variable
0 5 10 15
0 0.2 0.4 0.6 0.8 1
0 0.05 0.1 0.15 0.2 0.25 0.3 0.35

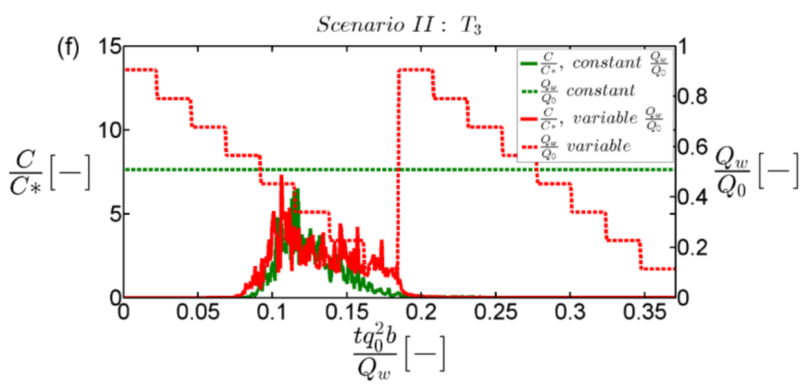
$Scenario\ II:\ T_3$
(f)
$\frac{C}{C*}[-]$
$\frac{Q_w}{Q_0}[-]$
$\frac{tq_0^2b}{Q_w}[-]$
$\frac{C}{C*}$, constant $\frac{Q_w}{Q_0}$
$\frac{Q_w}{Q_0}$ constant
$\frac{C}{C*}$, variable $\frac{Q_w}{Q_0}$
$\frac{Q_w}{Q_0}$ variable
0 5 10 15
0 0.2 0.4 0.6 0.8 1
0 0.05 0.1 0.15 0.2 0.25 0.3 0.35

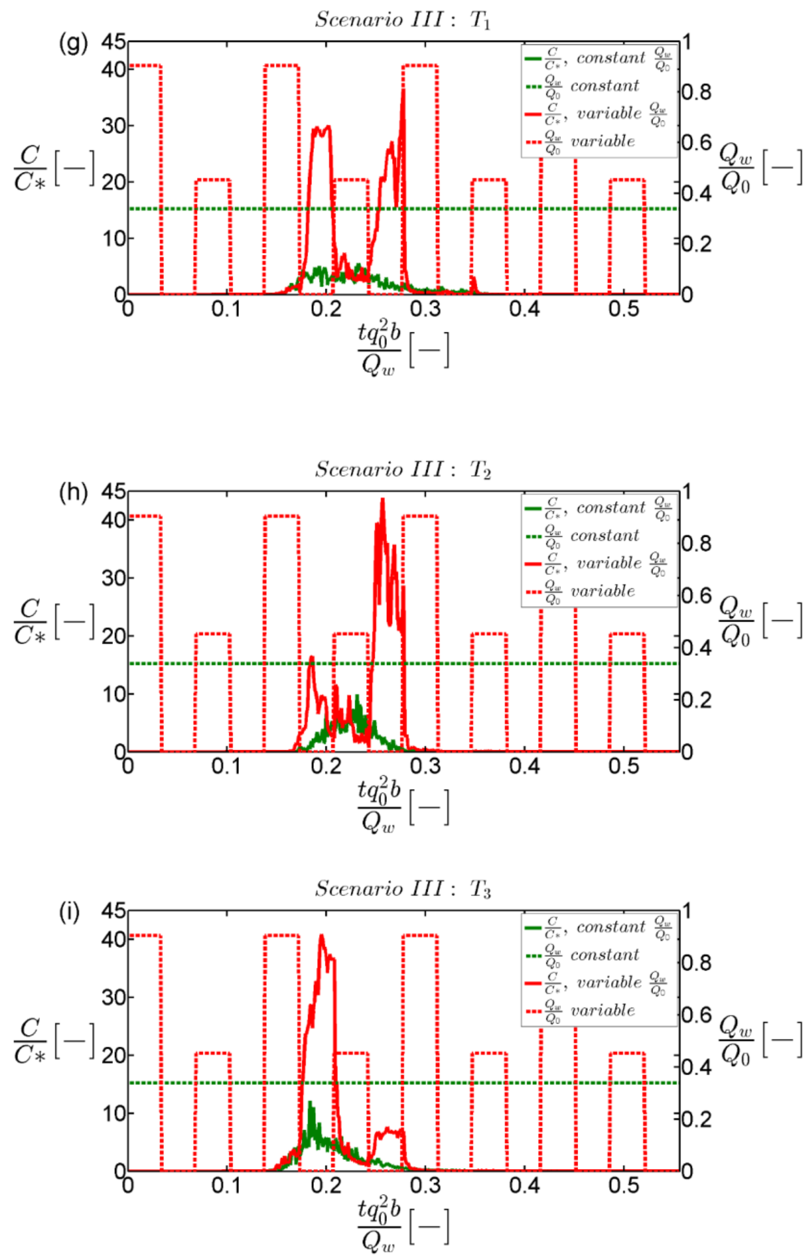

Fig. 3. Contaminant concentration BTCs observed at the pumping well for the three scenarios analyzed: Scenario I (plots a, b, c); Scenario II (plots d, e, f); and Scenario III (plots g, h, i).

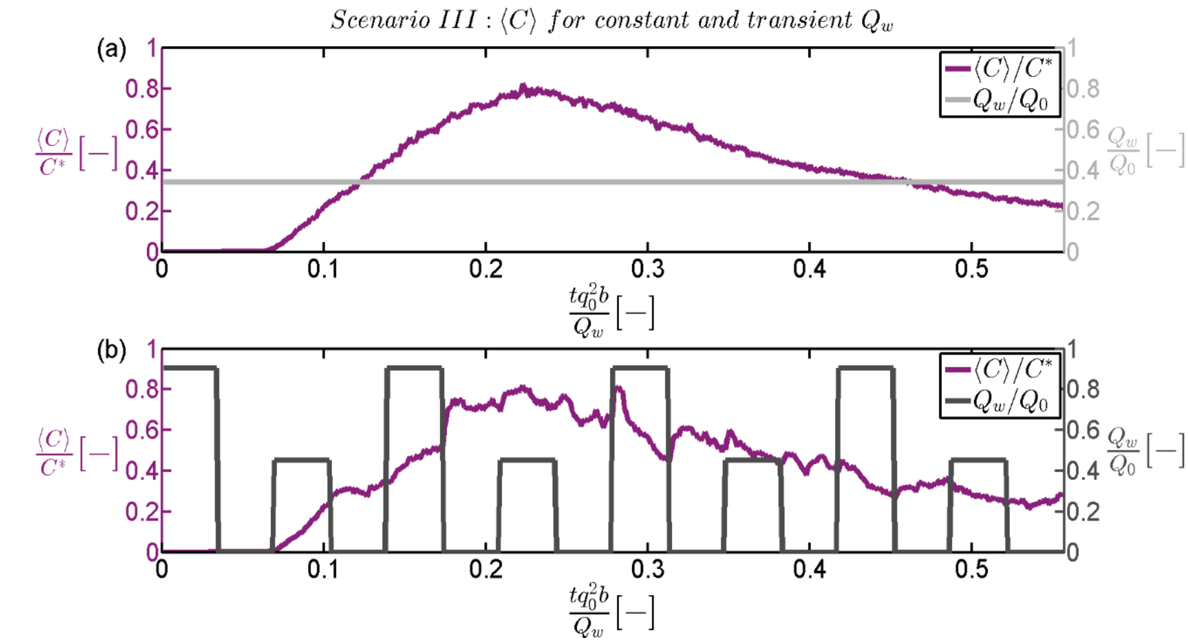

Fig. 4. Mean concentration $\langle C \rangle$ observed at the pumping well for the uniform pumping strategy of Scenario III (a) and the transient pumping strategy of Scenario III (b).

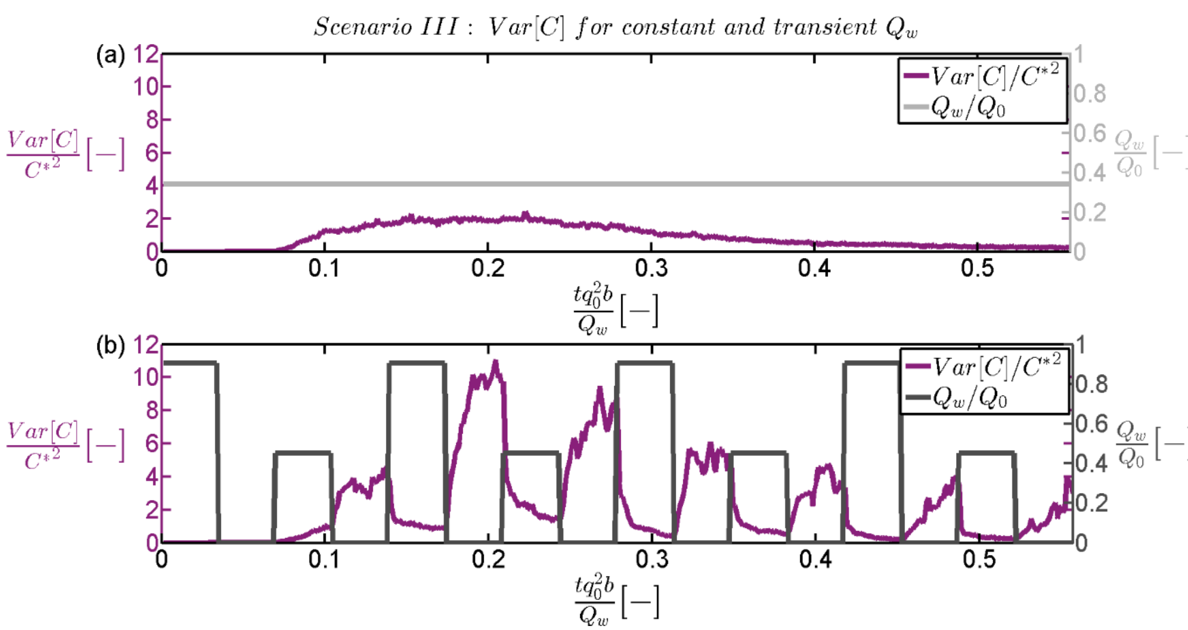

Fig. 5. Variance of the concentration $Var[C]$ observed at the pumping well for the uniform pumping strategy of Scenario III (a) and the transient pumping strategy of Scenario III (b).

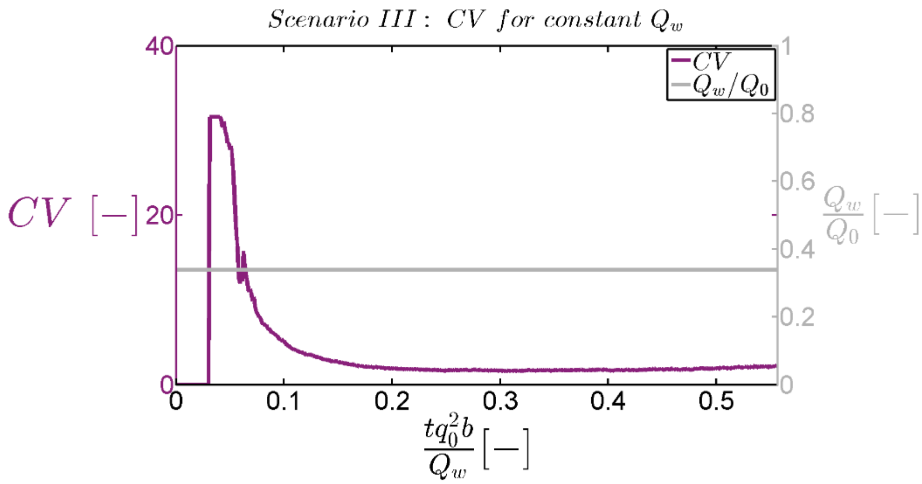

Fig. 6. Coefficient of variation *CV* of the concentration observed at the pumping well for the uniform pumping strategy of Scenario III.

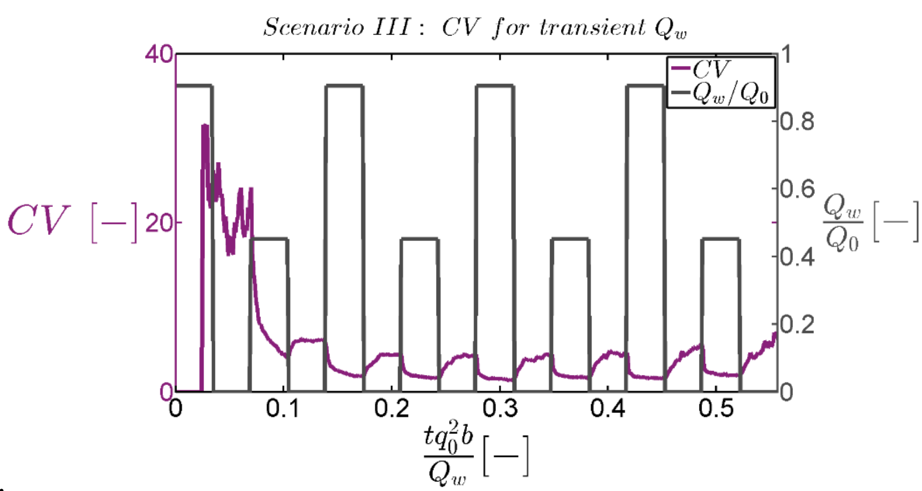

.

Fig. 7. Coefficient of variation *CV* of the concentration observed at the pumping well for the transient pumping strategy of Scenario III.

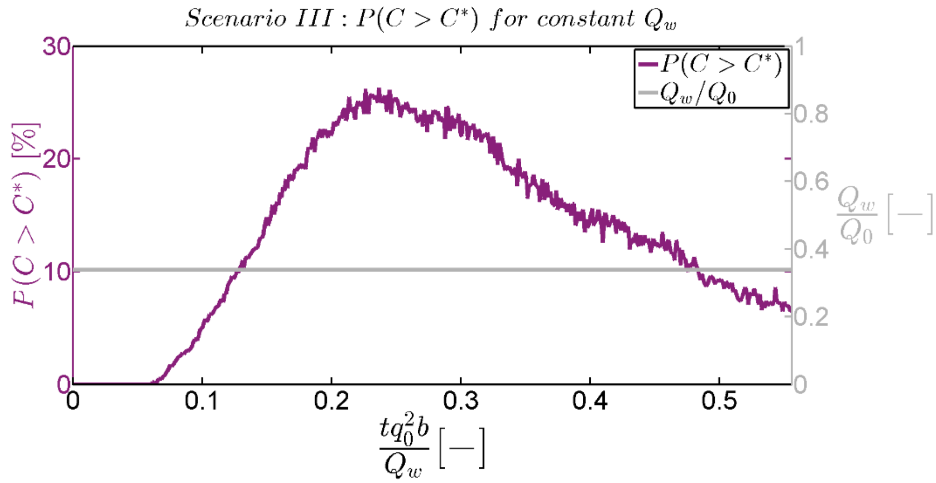

Fig. 8. Probability of exceedance of the concentration threshold $P(C > C^*)$ for the uniform pumping strategy of Scenario III.

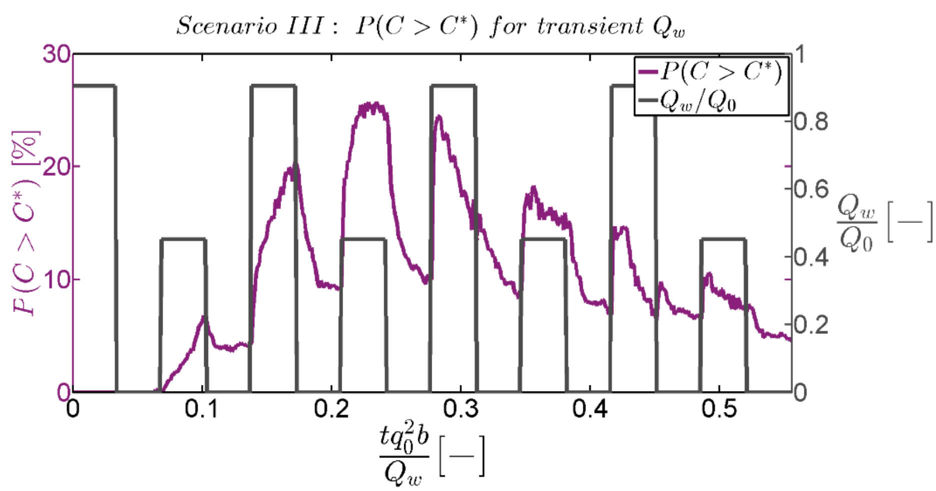

Fig. 9. Probability of exceedance of the concentration threshold $P(C > C^*)$ for the transient pumping strategy of Scenario III.

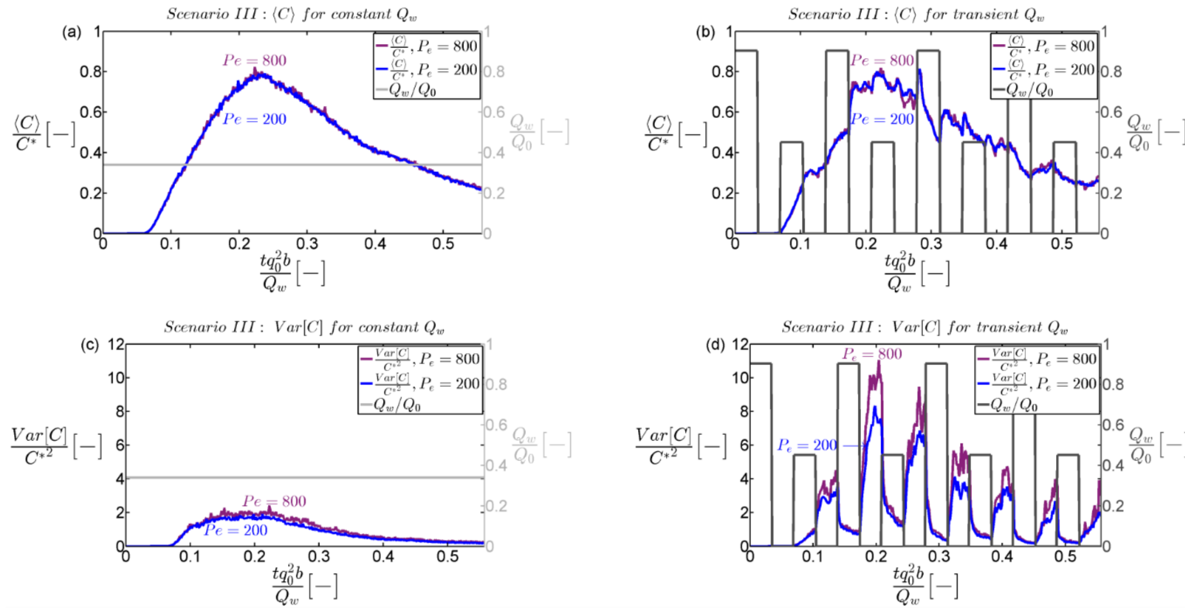

Fig. 10. Impact of the Péclet number (P_e) on the concentration mean for (a) constant and (b) time-varying pumping rate. Impact of the Péclet number (P_e) on the concentration variance for (c) constant and (d) time-varying pumping rate. Purple curves refer to P_e = 800 and blue curves refer to P_e = 200.

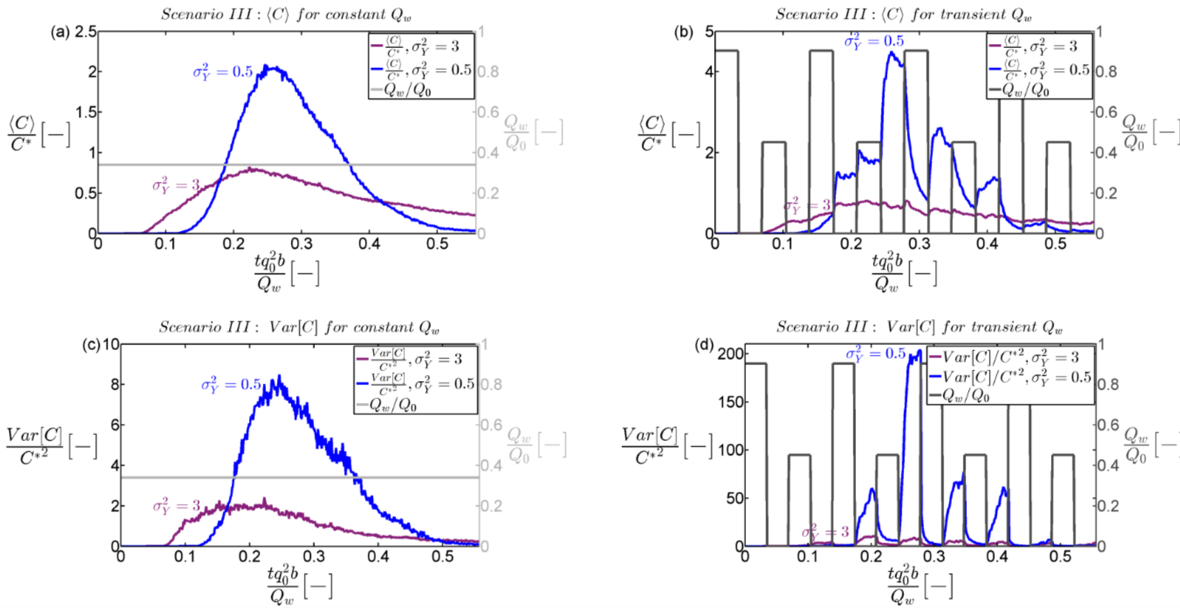

Fig. 11. Mean concentration for (a) constant and (b) time-varying pumping rates. Variance behavior is also depicted for (c) constant and (d) time-varying pumping schemes. Blue curves refer to low heterogeneity and purple curves to high heterogeneity.

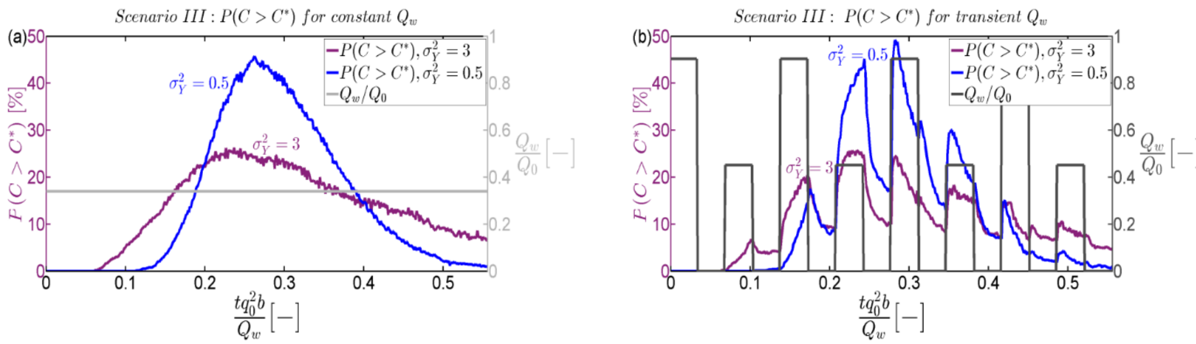

Fig. 12. Probability of exceedance of the concentration threshold $P(C > C^*)$ for (a) constant and (b) time-varying pumping rates. Blue curves refer to low heterogeneity and purple curves to high heterogeneity.

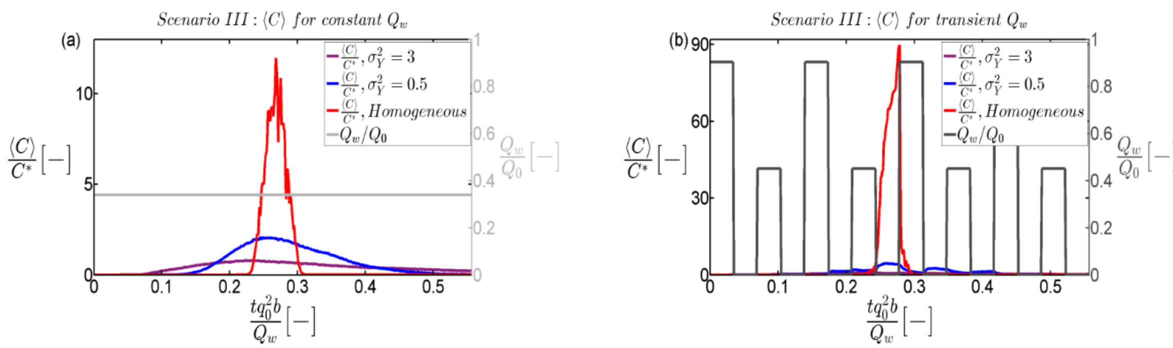

Fig. 13. Mean concentration $\langle C \rangle$ observed at the pumping well for (a) constant and (b) time-varying pumping strategy of Scenario III for different levels of aquifer heterogeneity.

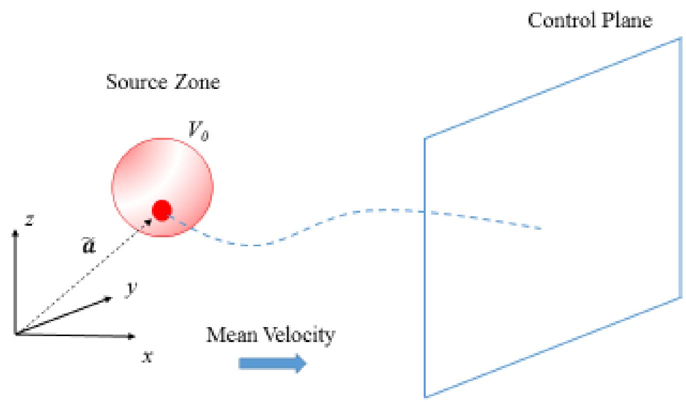

Fig. A.1. Schematic representation of the problem analyzed using the Lagrangian framework.

.